Original Article

Radiomic features from computed tomography to differentiate invasive pulmonary adenocarcinomas from non-invasive pulmonary adenocarcinomas appearing as part-solid ground-glass nodules

Ting Luo[1*], Ke Xu[1*], Zheng Zhang[1], Lina Zhang[1], Shandong Wu[2]

[1]Department of Radiology, the First Affiliated Hospital of China Medical University, Shenyang 110000, China; [2]Departments of Radiology, Biomedical Informatics, Bioengineering, and Intelligent Systems, University of Pittsburgh, Pittsburgh 15106, USA

*These authors contributed equally to this work.

Correspondence to: Lina Zhang, PhD. Department of Radiology, The First Affiliated Hospital of China Medical University, Shenyang 110000, China. Email: zhanglnda@163.com.

Abstract

Objective: We aim to investigate radiomic imaging features extracted in computed tomography (CT) images to differentiate invasive pulmonary adenocarcinomas (IPAs) from non-IPAs appearing as part-solid ground-glass nodules (GGNs), and to incorporate significant radiomic features with other clinically-assessed features to develop a diagnostic nomogram model for IPAs.

Methods: This retrospective study was performed, with Institutional Review Board approval, on 88 patients with a total of 100 part-solid nodules (56 IPAs and 44 non-IPAs) that were surgically confirmed between February 2014 and November 2016 in the First Affiliated Hospital of China Medical University. Quantitative radiomic features were computed automatically on 3D nodule volume segmented from arterial-phase contrast-enhanced CT images. A set of regular risk factors and visually-assessed qualitative CT imaging features were compared with the radiomic features using logistic regression analysis. Three diagnostic models, i.e., a basis model using the clinical factors and qualitative CT features, a radiomics model using significant radiomic features, and a nomogram model combining all significant features, were built and compared in terms of receiver operating characteristic (ROC) curves. Decision curve analysis was performed for the nomogram model to explore its potential clinical benefit.

Results: In addition to three visually-assessed qualitative imaging features, another three quantitative features selected from hundreds of radiomic features were found to be significantly (all $P<0.05$) associated with IPAs. The diagnostic nomogram model showed a significantly higher performance [area under the ROC curve (AUC) =0.903] in differentiating IPAs from non-IPAs than either the basis model (AUC=0.853, $P=0.0009$) or the radiomics model (AUC=0.769, $P<0.0001$). Decision curve analysis indicates a potential benefit of using such a nomogram model in clinical diagnosis.

Conclusions: Quantitative radiomic features provide additional information over clinically-assessed qualitative features for differentiating IPAs from non-IPAs appearing as GGNs, and a diagnostic nomogram model including all these significant features may be clinically useful in preoperative strategy planning.

Keywords: Radiomics; lung; adenocarcinomas; tomography; X-ray computed

Submitted Jul 03, 2018. Accepted for publication Dec 17, 2018.
doi: 10.21147/j.issn.1000-9604.2019.02.07
View this article at: https://doi.org/10.21147/j.issn.1000-9604.2019.02.07

Introduction

In the multidisciplinary classification of lung adenocarcinomas in 2011 (1), adenocarcinoma *in situ* and minimally invasive adenocarcinoma were considered for sublobar resection due to their good prognosis, with a very high 5-year disease-free survival (DFS). However, lobectomy is still the standard surgical treatment for invasive pulmonary adenocarcinomas (IPAs) with worse prognosis (5-year DFS is 74.6%, even in stage IA). For precise surgery, an accurate diagnosis between IPAs and non-IPAs before surgery is becoming increasingly crucial (2,3). A number of studies have demonstrated correlations between computed tomography (CT) findings of part-solid ground-glass nodules (GGNs) with histopathology (4). While visual nodule evaluation on morphological signs in CT images is clinically useful, it is subject to variations in imaging interpretation, and visual assessment may only be able to identify limited imaging discriminators of nodules (5,6).

Radiomics was introduced as the extraction and analysis of large amounts of advanced quantitative imaging features with high throughput from medical images obtained with CT, positron emission tomography (PET) or magnetic resonance imaging (MRI) (7). Recent radiomics studies on investigating pulmonary nodules have shown promising performance for histological subtyping (8), gene expression (9), malignancy prediction (10), posttreatment prognosis (11) and so on. Little work however was reported on studying GGNs using radomics-based methods for outcome prediction (10).

In this study, we investigated radiomics imaging features, clinical risk factors and visually-assessed qualitative CT imaging features in differentiating IPAs from non-IPAs appearing as GGNs and developed a diagnostic nomogram model based on statistically significant features identified from these different sources of features.

Materials and methods

Study cohort

A radiologist retrospectively searched for individuals with GGNs identified on chest CT from February 2014 to November 2016, using the electronic medical records and the radiology informatics system of the hospital with the following steps: first, among inpatients in the Department of Thoracic Surgery, we selected all CT scans with the keywords "GGO", "GGN", "part-solid nodule", "non-solid nodule", "ground-glass opacity" and "ground-glass nodule" in the reports with the surgically confirmed pathological results available. A total of 660 patients with keywords "GGO", "GGN", "part-solid nodule", "non-solid nodule", "ground-glass opacity", "ground-glass nodule" in CT reports and pathologically proven lesions were selected. Then, 331 patients with CT scans acquired by a Dual Source CT scanner were selected. To keep uniform acquisition protocol and parameters, 121 patients with thin-section images (section thickness = 2 mm) were left. Then, two expert radiologists reviewed all the CT scans and excluded GGNs of lesions larger than 3 cm, leaving a total of 88 patients with 100 GGNs for further analysis (*Figure 1*). Discrepancies in interpretation between two observers were resolved by a third radiologist for consensus reading. Finally, 88 patients with 100 part-solid nodules (33–78 years old; mean age: 56.45±8.60 years) were enrolled in this study. There were 22 males (35–78 years old; mean age: 53.46±9.81 years) and 66 females (33–77 years old; mean age: 56.56±10.02 years). Note that we used a subset of 69 randomly selected nodules, out of the 100, for model development (training cohort), while the rest 31 unseen cases were used as an independent cohort for model testing (testing cohort). The Institutional Review Board (IRB) of the First Affiliated Hospital of China Medical

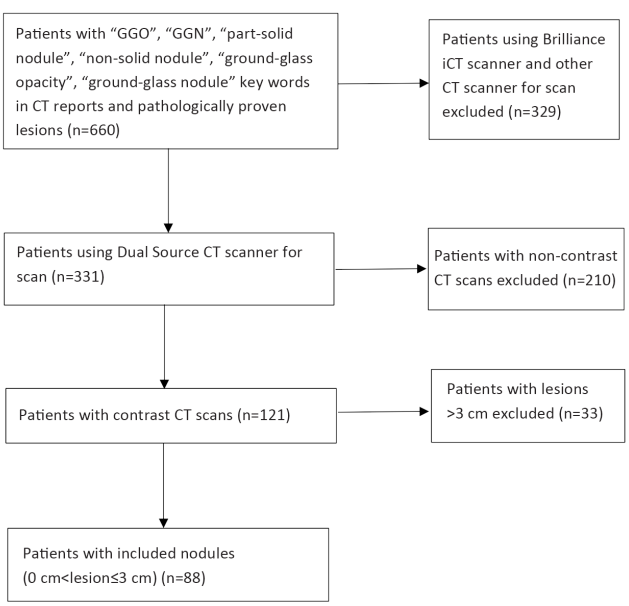

Figure 1 Flowchart of study population. Numbers in parentheses are the number of patients. CT, computed tomography.

University approved this retrospective study.

CT imaging protocol

All patients received contrast-enhanced chest CT using the same Dual Source CT scanner (Somatom Definition Flash, Siemens Medical Solutions, Forchheim, Germany). The acquisition parameters were as follows: 100 and 140 kV; CARE Dose 4D; 0.5 or 0.28 s rotation time; detector collimation, 128×0.5 mm; field of view, 350 mm × 350 mm; and matrix: 512×512. After routine non-enhanced CT, arterial-phase contrast-enhanced CT was performed after 10–15 s of intravenous administration of 70–90 mL of iodinated contrast material at a rate of 2.5–3.0 mL/s with a pump injector (Tennessee-XD2003, Ulrich Medical, Ulm, Germany). Contrast-enhanced CT was reconstructed with a construction thickness of 2 mm, a reconstruction interval of 2 mm, and a reconstruction kernel of D33f med smooth. CT scans were obtained for all patients in the supine position at full inspiration.

Clinical risk factors and visually-assessed qualitative CT imaging features

The first set of features is typical risk factors including age, gender, family history and smoking history. The second set of features is those visually-assessed qualitative CT imaging features that are used in current clinical diagnosis, including shape, margin, location, lesion size, pleural indentation, dilated bronchioles, vessel dilatation, solid component size and solid component proportion. All those risk factors and qualitative features were retrospectively extracted from clinical reports.

Quantitative radiomic features and a radiomics model

The third set of features is hundreds of quantitative radiomic features extracted from nodules. Nodules were first segmented manually by radiologists, by drawing a region of interest (ROI) along the boundary of each nodule on the CT images slice by slice until the entire nodule had been covered, yielding a three-dimensional nodule segmentation. A total of 396 commonly reported radiomic features (*Figure 2*), including morphological and textual structure descriptors, were computed automatically from the three-dimensional nodule volume, using the A.K. software (Analysis-Kinetics, GE Healthcare, USA).

Intra- and inter-reader reproducibility in nodule delineation

Radiomic features were computed from the nodule ROIs manually delineated by radiologists in CT images. The delineation of ROIs may introduce reader variations. The reader reproducibility of the ROI delineation was analyzed on 15 randomly selected patients (10 IPA and 5 non-IPA patients). First, two radiologists completed the ROI delineation on 15 patients independently without any information regarding the patients. Then, one radiologist (reader 1) repeated the ROI delineation after one week since the first round delineation, following the same procedure. An independent samples *t*-test or Kruskal-Wallis H test, where appropriate, was used to assess the differences between the computed radiomic features inside

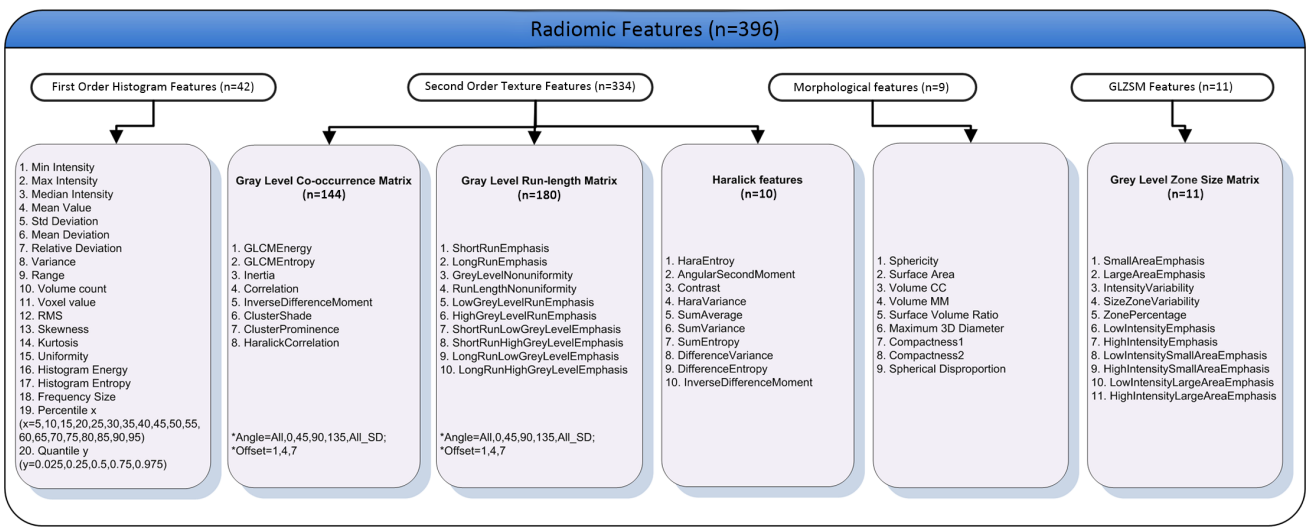

Figure 2 Quantitative radiomic features used in the study.

the delineated ROI. The intra-reader (reader 1 twice) and inter-reader (reader 1 *vs*. reader 2) reproducibility were evaluated by the intra- or inter-class correlation coefficients (ICCs), with a value greater than 0.75 indicating an acceptable agreement (12).

Statistical analysis and diagnostic/prediction modeling

We built three diagnostic/prediction models: a basis model, a radiomics model and a nomogram model, as described in the following. Area under the ROC curve (AUC) was used to assess the model performance. Z test was used to compare the AUC among the three models.

The basis model was based on the clinical risk factors and visually-assessed qualitative CT imaging features. Differences in each of these features between the IPAs and the non-IPAs were compared via univariate analysis using independent samples *t*-tests or the Kruskal-Wallis test as appropriate. A multivariate analysis was performed by the logistic regression model to build the basis model with the significant independent variables resulting from the univariate analysis.

The radiomics model was based on selected radiomic features alone. A univariate analysis, including a normality test, a homogeneity of variance test and a Kruskal-Wallis test, was performed to compare the differences in the quantitative radiomic features between the two groups (IPAs *vs*. non-IPAs) in the training cohort (the 69 patients for model development). Feature reduction was performed to remove features that were highly correlated with others (that is, if $|r|$ is equal to or greater than 0.90). Using the remaining features after feature reduction, logistic regression analysis was used to build the radiomics model to predict IPAs *vs*. non-IPAs. A radiomics score (denoted by Rad-score) was calculated for each patient by linearly combining the selected radiomic features weighted by each respective coefficient of the logistic regression model.

The nomogram model, built by multivariate logistic regression analysis, was based on the combination of the essential features selected/used in the basis model and the radiomics model. To evaluate the potential clinical diagnostic effects of the nomogram model, a decision curve analysis was performed, which quantified the net benefits of using such a model at different threshold probabilities (13).

All statistical analyses in this study were performed with R software (Version 3.3.3; R Foundation for Statistical Computing, Vienna, Austria, http://www.Rproject.org). A two-sided P value of less than 0.05 was considered statistically significant.

Results

Basis model

With regards to the clinical risk factors, there were no significant differences (P>0.05) for any of those factors between the IPAs and non-IPAs (*Table 1*). For qualitative CT imaging features, three significant features were identified: the univariate analysis showed that the IPAs were more frequently observed with greater solid component sizes (P=0.021 for training cohort; P=0.003 for testing cohort), higher solid component proportions (P=0.029 for training cohort; P=0.003 for testing cohort), and more pleural indentations (P=0.010 for training cohort; P=0.011 for testing cohort) than the non-IPAs (*Table 2*). The basis model based on solely the three significant features, i.e., pleural indentation, solid component size and solid component proportion, showed an AUC of 0.853 [95% confidence interval (95% CI): 0.698, 1.000] in distinguishing IPAs from non-IPAs appearing as GGNs (*Figure 3*).

Radiomics model

The inter-reader ICC of the radiomic features between reader 1 and reader 2 was 0.922. The intra-reader ICC for reader 1 was 0.915. Therefore, all analyses were based on the features extracted by reader 1. Out of the 396 radiomic features, 107 were significantly different between the IPA and non-IPA groups in univariate analysis. After feature reduction, three features (i.e., ClusterShade_angle45_

Table 1 Comparison of clinical risk factors between IPAs and non-IPAs

Characteristics	n (%)		P
	IPAs	Non-IPAs	
Age (year) ($\bar{x}\pm s$, range)	58±8 (42–78)	54±9 (33–74)	0.225
Gender			0.379
Male	15 (28.3)	7 (20.0)	
Female	38 (71.7)	28 (80.0)	
Family history			0.815
Yes	21 (39.6)	13 (37.1)	
No	32 (60.4)	22 (62.9)	
Smoking history			0.255
Yes	11 (20.8)	4 (11.4)	
No	42 (79.2)	31 (88.6)	

IPA, invasive pulmonary adenocarcinoma.

Table 2 Characteristics of visually-assessed qualitative CT imaging features between IPAs and non-IPAs both in training and testing cohorts

Characteristics	Training cohort			Testing cohort		
	IPAs	Non-IPAs	P	IPAs	Non-IPAs	P
Lesion size (cm) [median (25%, 75%)]	1.90 (1.30, 2.30)	1.50 (0.95, 2.13)	0.063	1.70 (1.50, 2.40)	1.05 (0.75, 1.93)	0.019
Solid component size (cm) [median (25%, 75%)]	0.86 (0.37, 1.16)	0.45 (0, 0.72)	0.021	0.78 (0.47, 0.84)	0 (0, 0.58)	0.003
Solid component proportion [median (25%, 75%)]	0.46 (0.27, 0.55)	0.29 (0, 0.48)	0.029	0.42 (0.24, 0.60)	0 (0, 0.28)	0.003
Shape [n (%)]			0.129			0.210
Round	14 (35.90)	18 (60.00)		10 (58.82)	9 (64.29)	
Lobular	10 (25.64)	4 (13.33)		5 (29.41)	1 (7.14)	
Irregular	15 (38.46)	8 (26.67)		2 (11.76)	4 (28.57)	
Lesion location [n (%)]			0.329			0.766
Superior lobe	30 (76.92)	20 (66.67)		8 (47.06)	8 (57.14)	
Middle lobe	4 (10.26)	2 (6.67)		2 (11.76)	2 (14.29)	
Interior lobe	5 (12.82)	8 (26.67)		7 (41.18)	4 (28.57)	
Margin [n (%)]			0.133			0.020
Blurred	9 (23.08)	13 (43.33)		5 (29.41)	2 (14.29)	
Spiculation	13 (33.33)	5 (16.67)		7 (41.18)	1 (7.14)	
Smooth	17 (43.59)	12 (40.00)		5 (29.41)	11 (78.57)	
Pleural indentation [n (%)]			0.010			0.011
Yes	21 (53.85)	25 (83.33)		7 (41.18)	12 (85.71)	
No	18 (46.15)	5 (16.67)		10 (58.82)	2 (14.29)	
Dilated bronchioles [n (%)]			0.217			0.409
Yes	9 (23.08)	11 (36.67)		6 (35.29)	7 (50.00)	
No	30 (76.92)	19 (63.33)		11 (64.71)	7 (50.00)	
Vessel dilatation [n (%)]			0.067			0.087
Yes	3 (7.69)	7 (23.33)		1 (5.88)	4 (28.57)	
No	36 (92.31)	23 (76.67)		16 (94.12)	10 (71.43)	

CT, computer tomography; IPA, invasive pulmonary adenocarcinoma.

offset7, sumEntropy, and Spherical Disproportion) were retained and used to build the radiomics model. The Rad-score, calculated as a single "overall" feature based on the weighted combination of the three radiomic features and corresponding logistic regression coefficients, was marginally significant (P=0.040) between the IPAs [mean Rad-score =1.037 (range: 0.326 to 2.587)] and non-IPAs [mean Rad-score = −0.536 (range: −1.385 to 0.096)]. The AUC of the radiomics model was 0.769 (95% CI: 0.601, 0.937) (*Figure 3*) in discriminating IPAs and non-IPAs appearing as GGNs.

Nomogram model

Multiple logistic regression analysis (*Table 3*) showed that the three qualitative CT imaging features [pleural indentation (P=0.006), solid component size (P=0.045) and solid component proportion (P=0.020)] and the quantitative Rad-score (P=0.046) were each significantly associated with IPAs. Their adjusted odds ratios were 7.189, 0.075, 194.786 and 2.016, respectively (*Table 3*). The diagnostic nomogram model (*Figure 4*) based on these four features showed an AUC of 0.903 (95% CI: 0.845, 0.975) (*Figure 3*).

In the result of Z test, the diagnostic nomogram model showed a significantly higher performance (AUC=0.903) in differentiating IPAs from non-IPAs than either the basis model (AUC=0.853, P=0.0009) or the radiomics model (AUC=0.769, P<0.0001).

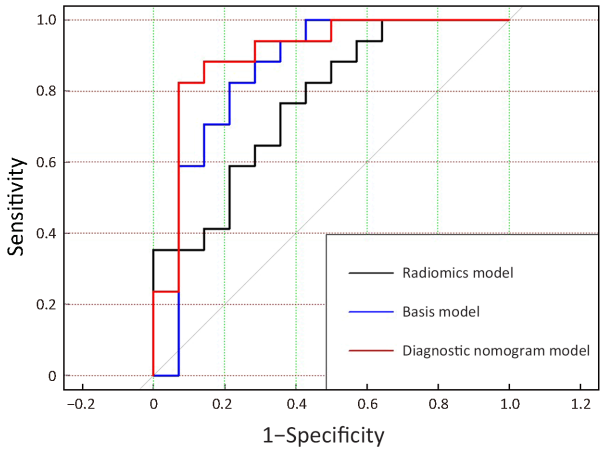

Figure 3 Receiver operating characteristic (ROC) curves of the basis model [area under the ROC curve (AUC)=0.853], radiomics model (AUC=0.769), and nomogram model (AUC=0.903). The nomogram model showed a significantly higher performance in differentiating invasive pulmonary adenocarcinomas (IPAs) from non-IPAs than either the basis model (P=0.0009) or the radiomics model (P<0.0001).

The decision curve analysis (*Figure 5*) indicated that the nomogram model would be more diagnostically beneficial in discriminating IPAs from non-IPAs, when the threshold probability falls in the range of 30%−90%.

Discussion

In this study, we investigated regular clinical risk factors, visually-assessed qualitative imaging features, and a large set of quantitative radiomic features in differentiating IPAs from non-IPAs using three models (basis model, radiomics model and nomogram model). Our results showed that the basis model outperforms the radiomics model and when their features are combined, the nomogram model performs better than either the basis or radiomics model. This finding indicates that radiomic features may provide additional information over the visually-assessed qualitative features for IPA diagnosis. Similar findings about the complementary effects of radiomic features were also reported in previous work (10). Based on the improved AUC performance, the nomogram model we built in this work may facilitate preoperative CT imaging interpretation for identifying IPAs from non-IPAs appearing as GGNs, and ultimately help better inform clinical treatment management of the disease.

The application of radiomic feature analysis has gained increased attention in recent years, as it may be suitable for assessing phenotypic heterogeneity of pulmonary nodules (14-17). Genomic heterogeneity within the volume of a pulmonary nodule is expected to be captured by phenotypic radiomics data such as the texture imaging features, enabling statistical evaluation of imaging data to obtain diagnostic, predicative or prognostic value (4,18). Reproducibility of quantitative radiomic features is critical for clinical/translational applications. While the calculations of all our radiomic features are automated, the segmentation of nodules was done manually by radiologists, which may introduce reader variations. Realizing that, we performed reproducibility experiments where both the intra- and inter-reader reproducibility of the ROI delineation is acceptable, providing additional robustness to the automated quantification of the radiomic features.

The significance of the three qualitative features, pleural indentations, solid component sizes and solid component proportions, is associated with clinical evaluations (19). The invasive components of the tumor, fibrotic proliferation or collapsed alveolar space often appear as the solid components of GGNs in CT images (20,21). There is a strong association between the diameter of the solid component on CT images and the invasive component as revealed by pathology (22). Moreover, the solid component size is a significant factor for prognosis (23) and DFS (24). In addition, the solid component proportion was also found to be a significant independent differentiator of IPAs from non-IPAs. A solid component proportion of ≥50% is

Table 3 Multivariate logistic regression analysis of four significant features

Intercept and variable	β	OR (95% CI)	P
Intercept	−0.729	0.482 (0.191, 1.220)	0.125
Rad-score	0.701	2.016 (1.012, 4.020)	0.046
Pleural indentation	1.973	7.189 (1.750, 29.500)	0.006
Solid component size	−2.590	0.075 (0.006, 0.941)	0.045
Solid component proportion	5.272	194.786 (2.290, 1,660.000)	0.020

OR, odds ratio; 95% CI, 95% confidence interval.

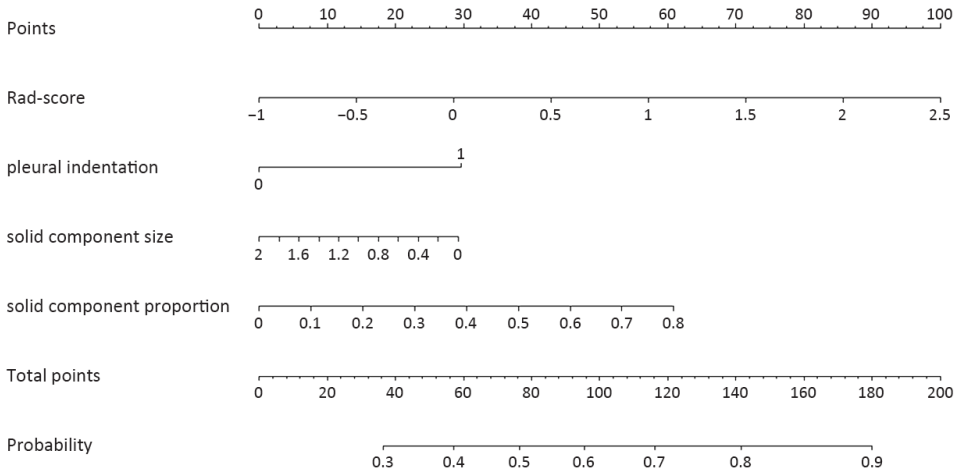

Figure 4 Diagnostic nomogram model based on the four significant features, Rad-score, pleural indentation, solid component size and solid component proportion.

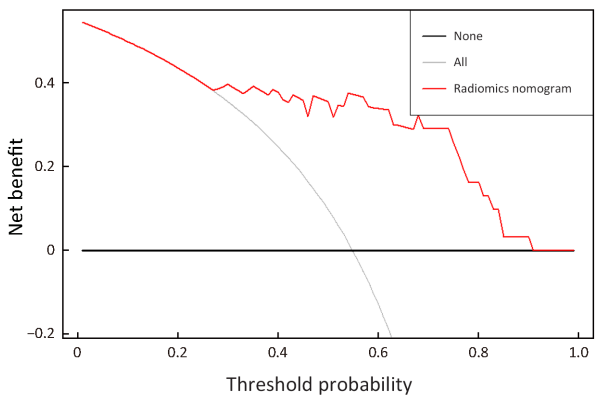

Figure 5 Decision curve analysis of diagnostic nomogram model. The gray line represents the assumption that all patients have invasive pulmonary adenocarcinomas (IPAs). The black line represents the assumption that no patient has an IPA. The red line represents the net benefit of using the nomogram model to diagnose/predict IPAs.

considered the cutoff value for invasiveness potential in pathology (3) and in lesions smaller than 3 cm with solid component proportions >50%, the rate of lymph node metastasis ranges from 21% to 26% (25-27). Pleural indentation on pulmonary CT images, representing fibrotic strands around the tumor as a result of central fibrosis and surrounding tissue contraction, is often found in malignant lesions (58%–93%) (28-30). In addition, the frequency of pleural indentation is significantly higher in malignant GGNs than in benign GGNs (70.5% *vs*. 4.8%, respectively), as reported by Fan *et al* (31). It has been inferred that this feature may be associated with intratumoral desmoplastic reactions (32). Nambu *et al*. also hypothesized that this may be attributed to the strong contraction of the solid component (33). It should be noted that in our study, the ROIs were delineated carefully on the nodule boundary without involving the pleural condition. Therefore, effective information characterized by the pleural conditions may not be completely captured by the radiomic features and thus the radiomics model. This may partly explain the complementary nature of the finally-selected significant qualitative CT features (pleural retractions, solid component sizes and solid component proportions) and quantitative radiomic features (i.e., Rad-scores) in the nomogram model. It therefore makes sense for us to integrate these four significant features to develop the nomogram model and the model showed an enhanced performance.

This study had several limitations. First, this is a retrospective single-institutional study with a moderate sample size of study cohort. We had to exclude a larger number of ineligible patients in order to largely reduce the potential confounding effects caused by difference in CT scanner, imaging protocol and lesion size. In the previous study, Mackin *et al*. found that the inter-scanner differences should be considered in assessing radiomic feature variability (34). Therefore, all the CT images included in our study were generated by the same CT scanner and the same acquisition protocol. Our study therefore represents a high scientific rigor in data analysis. We acknowledge that future larger studies are warranted to examine the findings

of our study in other similar patient cohorts. Second, nodule segmentation was done manually by radiologists, which is time-consuming and may introduce reader variations. Accurate and robust fully-automated computer algorithms for nodule segmentation are desired but currently not available to us. We believe that further development of such algorithms is needed in future work. Finally, the three qualitative imaging features included in the nomogram model are still subject to reader variations because they are assessed visually by radiologists. If more descriptive quantitative radiomic features can be designed/implemented to capture the essential information underlying those qualitative features, it may be possible to build an updated nomogram model using all quantitative radiomic features. This is one of the future works that we are going to explore.

Conclusions

We investigated quantitative radiomic imaging features in differentiating IPAs from non-IPAs appearing as GGNs in CT images. In our study cohort, we showed that radiomic features provide additional information over three visually-assessed qualitative CT imaging features. We built a diagnostic nomogram model by integrating all of these significant features and the model yielded an improved AUC than models using radiomics or qualitative features alone. While such diagnosis model may facilitate clinical applications in preoperative strategy planning, further evaluation of our findings and the models is required in future work.

Acknowledgements

This work was supported by the National Natural Science Foundation of China (No. 81301222), the Special Research Grant for Non-profit Public Service (No. 201402013), and the Science and Technology Department Project of Liaoning province (No. 2012020073-302). We sincerely appreciate Yan Guo and Xin Li from the Department of Core Imaging, Life Science, GE healthcare, Shanghai, China for their assistance in data processing and statistical analysis.

Footnote

Conflicts of Interest: The authors have no conflicts of interest to declare.

References

1. Travis WD, Brambilla E, Noguchi M, et al. International association for the study of lung cancer/American thoracic society/European respiratory society international multidisciplinary classification of lung adenocarcinoma. J Thorac Oncol 2011;6:244-85.
2. Akata S, Yoshimura M, Nishio R, et al. High-resolution computed tomographic findings of small peripherally located squamous cell carcinoma. Clin Imaging 2008;32:259-63.
3. Kobayashi Y, Sakao Y, Deshpande GA, et al. The association between baseline clinical-radiological characteristics and growth of pulmonary nodules with ground-glass opacity. Lung Cancer 2014;83:61-6.
4. Wilson R, Devaraj A. Radiomics of pulmonary nodules and lung cancer. Transl Lung Cancer Res 2017;6:86-91.
5. Revel MP, Bissery A, Bienvenu M, et al. Are two-dimensional CT measurements of small noncalcified pulmonary nodules reliable? Radiology 2004;231:453-8.
6. Revel MP, Merlin A, Peyrard S, et al. Software volumetric evaluation of doubling times for differentiating benign versus malignant pulmonary nodules. AJR Am J Roentgenol 2006;187:135-42.
7. Lambin P, Rios-Velazquez E, Leijenaar R, et al. Radiomics: extracting more information from medical images using advanced feature analysis. Eur J Cancer 2012;48:441-6.
8. Wu WM, Parmar C, Grossmann P, et al. Exploratory study to identify radiomics classifiers for lung cancer histology. Front Oncol 2016;6:71.
9. Liu Y, Kim J, Balagurunathan Y, et al. Radiomic features are associated with EGFR mutation status in lung adenocarcinomas. Clin Lung Cancer 2016;17:441-8.e6.
10. Lee SH, Lee SM, Goo JM, et al. Usefulness of texture analysis in differentiating transient from persistent part-solid nodules (PSNs): a retrospective study. PLoS One 2014;9:e85167.
11. Coroller TP, Agrawal V, Narayan V, et al. Radiomic phenotype features predict pathological response in non-small cell lung cancer. Radiother Oncol 2016;119:480-6.

12. Shrout PE, Fleiss JL. Intraclass correlations: uses in assessing rater reliability. Psychol Bull 1979;86:420-8.
13. Vickers AJ, Cronin AM, Elkin EB, et al. Extensions to decision curve analysis, a novel method for evaluating diagnostic tests, prediction models and molecular markers. BMC Med Inform Decis Mak 2008;8:53.
14. Hawkins S, Wang H, Liu Y, et al. Predicting malignant nodules from screening CT scans. J Thorac Oncol 2016;11:2120-8.
15. Chae HD, Park CM, Park SJ, et al. Computerized texture analysis of persistent part-solid ground-glass nodules: differentiation of preinvasive lesions from invasive pulmonary adenocarcinomas. Radiology 2014;273:285-93.
16. Colen R, Foster I, Gatenby R, et al. NCI workshop report: clinical and computational requirements for correlating imaging phenotypes with genomics signatures. Transl Oncol 2014;7:556-69.
17. Parmar C, Leijenaar RT, Grossmann P, et al. Radiomic feature clusters and prognostic signatures specific for Lung and Head & Neck cancer. Sci Rep 2015;5:11044.
18. Lambin P, Leijenaar RTH, Deist TM, et al. Radiomics: the bridge between medical imaging and personalized medicine. Nat Rev Clin Oncol 2017; 14:749-62.
19. Lee SM, Park CM, Goo JM, et al. Invasive pulmonary adenocarcinomas versus preinvasive lesions appearing as ground-glass nodules: differentiation by using CT features. Radiology 2013;268:265-73.
20. Noguchi M, Morikawa A, Kawasaki M, et al. Small adenocarcinoma of the lung. Histologic characteristics and prognosis. Cancer 1995;75:2844-52.
21. Park CM, Goo JM, Lee HJ, et al. Nodular ground-glass opacity at thin-section CT: histologic correlation and evaluation of change at follow-up. Radiographics 2007;27:391-408.
22. Lee KH, Goo JM, Park SJ, et al. Correlation between the size of the solid component on thin-section CT and the invasive component on pathology in small lung adenocarcinomas manifesting as ground-glass nodules. J Thorac Oncol 2014;9:74-82.
23. Sakao Y, Nakazono T, Tomimitsu S, et al. Lung adenocarcinoma can be subtyped according to tumor dimension by computed tomography mediastinal-window setting. Additional size criteria for clinical T1 adenocarcinoma. Eur J Cardiothorac Surg 2004; 26:1211-5.
24. Tsutani Y, Miyata Y, Nakayama H, et al. Prognostic significance of using solid versus whole tumor size on high-resolution computed tomography for predicting pathologic malignant grade of tumors in clinical stage IA lung adenocarcinoma: a multicenter study. J Thorac Cardiovasc Surg 2012;143:607-12.
25. Aoki T, Tomoda Y, Watanabe H, et al. Peripheral lung adenocarcinoma: correlation of thin-section CT findings with histologic prognostic factors and survival. Radiology 2001;220:803-9.
26. Matsuguma H, Yokoi K, Anraku M, et al. Proportion of ground-glass opacity on high-resolution computed tomography in clinical T1 N0 M0 adenocarcinoma of the lung: A predictor of lymph node metastasis. J Thorac Cardiovasc Surg 2002;124:278-84.
27. Nakata M, Sawada S, Yamashita M, et al. Objective radiologic analysis of ground-glass opacity aimed at curative limited resection for small peripheral non-small cell lung cancer. J Thorac Cardiovasc Surg 2005;129:1226-31.
28. Takashima S, Maruyama Y, Hasegawa M, et al. CT findings and progression of small peripheral lung neoplasms having a replacement growth pattern. AJR Am J Roentgenol 2003;180:817-26.
29. Kuriyama K, Tateishi R, Doi O, et al. CT-pathologic correlation in small peripheral lung cancers. AJR Am J Roentgenol 1987;149:1139-43.
30. Zwirewich CV, Vedal S, Miller RR, et al. Solitary pulmonary nodule: high-resolution CT and radiologic-pathologic correlation. Radiology 1991; 179:469-76.
31. Fan L, Liu SY, Li QC, et al. Multidetector CT features of pulmonary focal ground-glass opacity: differences between benign and malignant. Br J Radiol 2012;85:897-904.
32. Zhang Y, Shen Y, Qiang JW, et al. HRCT features distinguishing pre-invasive from invasive pulmonary adenocarcinomas appearing as ground-glass nodules. Eur Radiol 2016;26:2921-8.
33. Nambu A, Araki T, Taguchi Y, et al. Focal area of ground-glass opacity and ground-glass opacity

predominance on thin-section CT: discrimination between neoplastic and non-neoplastic lesions. Clin Radiol 2005;60:1006-17.

34. Mackin D, Fave X, Zhang L, et al. Measuring computed tomography scanner variability of radiomics features. Invest Radiol 2015;50:757-65.

Cite this article as: Luo T, Xu K, Zhang Z, Zhang L, Wu S. Radiomic features from computed tomography to differentiate invasive pulmonary adenocarcinomas from non-invasive pulmonary adenocarcinomas appearing as part-solid ground-glass nodules. Chin J Cancer Res 2019;31(2):329-338. doi: 10.21147/j.issn.1000-9604.2019.02.07

